JAK/STAT3 Pathway Promotes Proliferation of Ovarian Aggregate-derived Stem Cells in vitro

Maryam Saber
Department of Stem Cells and Developmental Biology, Cell Science Research Center, Royan Institute for Stem Cell Biology and Technology, ACECR, Tehran, Iran

Faezeh Shekari
Department of Stem Cells and Developmental Biology, Cell Science Research Center, Royan Institute for Stem Cell Biology and Technology, ACECR, Tehran, Iran

Seyed-Ahmad Mousavi
Department of Stem Cells and Developmental Biology, Cell Science Research Center, Royan Institute for Stem Cell Biology and Technology, ACECR, Tehran, Iran

Ashraf Moini
Department of Endocrinology and Female Infertility, Reproductive Biomedicine Research Center, Royan Institute for Reproductive Biomedicine, ACECR, Tehran, Iran

Monireh-Sadat Miri
Department of Stem Cells and Developmental Biology, Cell Science Research Center, Royan Institute for Stem Cell Biology and Technology, ACECR, Tehran, Iran

Fereshteh Esfandiari (fereshtehesfandiari@royaninstitute.org)
Department of Stem Cells and Developmental Biology, Cell Science Research Center, Royan Institute for Stem Cell Biology and Technology, ACECR, Tehran, Iran

---

Research Article

Keywords: Ovarian stem cells, Three-dimensional culture system, Aggregate, JAK/STAT3 signaling pathway

Posted Date: April 6th, 2022

DOI: https://doi.org/10.21203/rs.3.rs-1518202/v1

Abstract

Background

The accurate identification and isolation of ovarian stem cells from mammalian ovaries remain a major challenge because of the lack of specific surface markers and suitable *in vitro* culture systems. Optimized culture conditions for *in vitro* expansion of ovarian stem cells would allow for identifying requirements of these stem cells for proliferation and differentiation that would pave the way to uncover role of ovarian stem cells in ovarian pathophysiology. Here, we used three-dimensional (3D) aggregate culture system for enrichment of ovarian stem cells and named them aggregate-derived stem cells (ASCs). We hypothesized that mimicking the ovarian microenvironment *in vitro* by using an aggregate model of the ovary would provide a suitable niche for the isolation of ovarian stem cells from adult mouse and human ovaries and wanted to find out the main cellular pathway governing the proliferation of these stem cells.

Results

We showed that ovarian aggregates take an example from ovary microenvironment in terms of expression of ovarian markers, hormone secretion and supporting the viability of the cells. We found that aggregates-derived stem cells proliferate *in vitro* as long-term while remained expression of germline markers. These ovarian stem cells differentiated to oocyte like cells *in vitro* spontaneously. Transplantation of these stem cells in to chemotherapy mouse ovary could restore ovarian structure. RNA-sequencing analysis revealed that interleukin6 is upregulated pathway in ovarian aggregate-derived stem cells. Our data showed that JAK/Stat3 signaling pathway which is activated downstream of IL6 is critical for ovarian stem cells proliferation.

Conclusions

We developed a platform that is highly reproducible for *in vitro* propagation of ovarian stem cells. Our study provides a primary insight into cellular pathway governing the proliferation of ovarian stem cells.

Introduction

Various tissues in the body contain populations of stem cells that may be quiescent or actively divid (1, 2). The proliferation property of stem cells varies in various tissues; Stem cells in skin, stomach, intestine, bone marrow, and the hematopoietic system have extensively capacity of proliferation (3). To date, very little is known about the nature and localization of stem cells in mammalian female reproductive tract and in especially in the ovary (3, 4). Recent evidences support the existence of stem cells including theca stem cells(5, 6), very small embryonic-like stem cells (VSELs) (7) and oogonial stem cells (OSCs) (8, 9) within the ovary. The mammalian ovary undergoes cyclic ovulatory rupture and repair every month. This

remarkable cyclic regenerative capacity of the ovarian surface epithelium suggests the existence of resident stem cells (6, 10, 11).

Most stem-cell enrichment protocols rely on immune sorting, and use sets of antibodies to surface proteins on the target cells(12–14). However, the isolation of stem cells from the ovary in humans and rodents has been hindered by the lack of cell-surface markers specific for ovarian stem cells, and by the lack of suitable in vitro culture systems which maintain these cells in an undifferentiated state and testing the stem cell properties(15, 16). Recent approaches in three-dimensional (3D) cultures relies on the assumption that the fate of stem cells and the cell cycle are controlled by interactions between the cells and their particular microenvironment, known as stem cell niche(17–19). These culture systems are being widely used for enrichment of stem-like cells(14, 20). This approach have been recently used for propagation of stem cells in many adult epithelial system, including the mammary gland(13) and prostate(21). In this approach, using the elimination of the constraint of a niche that leads to quiescent stem cells *in vivo*(22), cells undergo cell division in 3D matrix culture (both symmetric and asymmetric), generating both stem and progenitor cells that rapidly reproduce toward the lineage commitment(14, 23, 24). Therefore, we hypothesized that an 3D culture approach composed of ovarian cells (without mature oocytes) would provide a suitable environment for the isolation of presumptive ovarian stem cells from adult mouse and human ovaries. We developed a 3D culture from ovarian cells that generated ovarian aggregates and assessed the characteristics of aggregated derived stem cells (ASCs) which were emerged in this platform. Next, we investigated the intrinsic nature of these cells and found that the Janus kinases (JAKs)/signal transducer and activator of transcription proteins (JAK/STAT3) signaling pathway is involved in self-renewal of ASCs. It is known that the JAK/STAT3 signaling pathway is crucial for maintenance of pluripotency in embryonic stem cells(25) but to our best knowledge, this is a first evidence regarding the effects of the JAK/STAT3 pathway on proliferation of ASCs.

Materials And Methods

Animals

Wild-type adult female NMRI mice (6–8 weeks old) were purchased from Pasteur Institute (Tehran, Iran). The female mice were used for ovarian cell isolation of ovarian tissues. The nude female mice that were used in the transplantation experiments and teratoma assessments were obtained from Pasteur Institute (Tehran, Iran). All animals were maintained on a 12 h light-dark cycle with access to water and standard chow ad libitum. The Royan Institutional Review Board and Institutional Ethical Committee of Royan Institute approved all animal care studies and procedures (No: Ec/92/1026).

Mice ovarian cell isolation

For each experiment, we collected ovarian tissues from 4 mice (8 ovaries). The fat pad, bursa, and oviduct were carefully removed from each of the ovarian tissues. Then, the ovaries were minced and washed twice in Hank's balanced salt solution (HBSS, Sigma-Aldrich) that contained 1% penicillin and streptomycin (Invitrogen). Ovarian tissues underwent enzymatic digestion along with a gentle hand

orbital shaking at 37°C in a water bath for 10 min in a solution of 2 ml HBSS that included 800 U/ml of type IV collagenase (Invitrogen) and 1 µg/ ml DNase I (Sigma-Aldrich). Because of the influence of mechanical stress on cell viability during isolation (26), we did not use from orbital shaker for ovarian cell dissociation, that led to increased cell viability and later aggregate formation (data not shown). Moreover, stem cells are sensitive to enzymes (27), therefore, fresh enzyme solution was prepared for each experiment. We replaced 1.5 ml of the supernatant with 1.5 ml fresh enzyme solution and continued the procedure until the majority of the ovarian tissues were dissociated (Supplementary Fig. 1). The collected supernatants were kept on ice for each repeat of the procedure. Finally, the supernatants collected from all of the procedures were filtered through a 40 µm nylon mesh and centrifuged at 300 g for 5 min, then washed twice with HBSS. The supernatant was removed carefully and the clumps of cells were resuspended in culture medium.

Human ovarian tissues

Human ovarian tissue samples were obtained after provision of written informed consent from eight reproductive age women (35–45 years of age) who presented for treatment of uterine disorders. These women were candidates for either a myomectomy or hysterectomy due to various reasons that included uterine fibroids which caused pain and bleeding or they were candidates for tubectomy for blocked fallopian tubes. Each woman signed an informed consent for participation and a questionnaire that recorded sex, age, and medical history was completed at the time of enrollment. The Royan Institutional Review Board and Institutional Ethical Committee of Royan Institute (No: Ec/92/1026) approved the use and preparation of the human ovarian samples for this study.

Human ovarian cell isolation

Biopsies of the human ovary tissues (2×2×2 cm) were transported in α-MEM media that contained penicillin (100 U/ml) and streptomycin (100 µg/ml) (both from Invitrogen) on ice to the laboratory. The biopsies were gently washed several times in HBSS that contained antibiotics. The ovarian tissues were dissected and minced by a sterile surgical instrument and rinsed with HBSS. Tissue dissociation was performed by using the enzymatic digestion method described for mice ovaries.

Aggregate formation

We seeded the single cells on agarose-coated plates to generate ovarian aggregates from the ovarian cells. For optimization of cell seeding, we used 1×10^5–5×10^5 cells per 3 cm^2 plate in 2 ml medium and observed that 3×10^5 cells/3 cm^2 plate (Falcon) were suitable for aggregate formation over 2–3 days of culture (data not shown). Seeding less than 3×10^5 cells decreased both the size and number of the aggregates, and resulted in their gradual degeneration. Aggregate formation with higher numbers of cultured cells joined together after 24 h and formed more dense aggregates. The cells were seeded on plates precoated with 1% agarose and incubated at 37°C and 5% CO_2 in α-MEM (Invitrogen) supplemented with 10% FBS (Hyclone), 1 mM sodium pyruvate (Invitrogen), 1 mM nonessential amino acids (Invitrogen), 2 mM L-glutamine (Sigma), 1X penicillin-streptomycin (Invitrogen), 0.1 mM β-

mercaptoethanol (Sigma-Aldrich), 1% N2 supplement (R&D), 10^3 units/ml leukemia inhibitory factor (LIF, Royan BioTech), 10 ng/ml recombinant human epidermal growth factor (rhEGF, Royan BioTech), 1 ng/ml basic fibroblast growth factor (bFGF, Royan BioTech), and 40 ng/ml glial cell-derived neurotropic factor (GDNF, Royan BioTech). After 2–3 days of cell culture, we observed the formation of round or oval aggregates of ovarian cells that were 50–100 μm in diameter.

In vitro derivation and expansion of ASCs

The aggregates were collected using a thin Pasteur pipette and plated in 12-well plates (approximately 5 aggregates per well). The 12-well plates were precoated with mitotically inactivated mouse embryonic fibroblasts (MEF), which were treated with mitomycin (Sigma-Aldrich). After three days, we observed the appearance of round cells that migrated from the aggregates and expanded in the culture. These cells were similar in size and morphology to the previously reported germline stem cells by White et al.(9).

The ASCs proliferated in culture over time. The medium was renewed every 2–3 days. The mice ASCs were passaged initially at a 1:2 split ratio with 0.05% trypsin-EDTA (Invitrogen) and re-plated on fresh MEF; after 4–5 passages, they were split at a 1:3 ratio. The human ASCs were passaged every 30 days with a split ratio of 1:2.

In vitro differentiation of ASCs into oocyte-like cells

Spherical oocyte-like cells (OLCs) spontaneously formed in culture during *in vitro* expansion of the ASCs. For directed oocyte differentiation, we cultured the ASCs in differentiation medium that contained α-MEM supplemented with 10% FBS, 1 mM sodium pyruvate, 1 mM nonessential amino acids, 2 mM L-glutamine, 1X concentrated penicillin-streptomycin, 0.1 mM β-mercaptoethanol, 1% N2 supplement (R&D), 10 ng/ml rhEGF, 5 μl/ml insulin/transferrin/selenium (Invitrogen), 0.05 IU follicle stimulating hormone (FSH; Sigma-Aldrich), and 0.03 IU luteinizing hormone (LH; Sigma-Aldrich). Each 2–3 days we replaced half of the medium with fresh medium. Supplementary Material Table S3 lists the differentiation media.

ASCs cryopreservation

The ASCs were trypsinized and gently mixed with cryoprotective solution (90% FBS and 10% DMSO), incubated overnight at -80°C, and then transferred to liquid nitrogen.

Flow cytometry

We performed flow cytometry analysis to assess the effects of cryopreservation on ASCs viability. Propidium iodide (PI) was used to detect the nonviable cells. Cells before and after cryopreservation were incubated with 0.05% trypsin-EDTA at 37°C for 3 min to obtain a single-cell suspension. We added PI to the cell suspension just prior to FACS analysis to enable detection of any nonviable cells by the BD FACS Aria II.

Reverse transcription-polymerase chain reaction (RT-PCR) analyses

Total RNA was extracted with TRIzol reagent (Invitrogen) according to the manufacturer's protocol. Reverse transcription was performed using the cDNA Synthesis Kit (K1632, Fermentas). The presence of each indicated mRNA was analyzed by conventional RT-PCR using the primers listed in Table S1.

Measurements of 17 β-estradiol and inhibin

We evaluated the endocrine functions of ovarian cells in the aggregates by measuring the levels of 17 β-estradiol (E2) and inhibin in the culture media. Ovarian cells were cultured in the presence and absence of 0.01 IU FSH and 7.5 IU LH for two days under 3D culture conditions. The culture media was collected to assess the secretion of these hormones with an ELISA kit (Shanghai Crystal Day Biotech Co., Ltd.) according to the manufacturer's instructions.

Alkaline phosphatase

We used an Alkaline Phosphatase Staining Kit (Sigma-Aldrich) to detect alkaline phosphatase (AP) activity in the ASCs. Mouse embryonic stem cells (mESCs) were used as the positive control.

Immunocytofluorescence staining

aggregate-derived cells were washed with 1X-concentrated phosphate-buffered saline (PBS) and fixed in 4% PFA for 20 min. After permeabilization with 0.5% Triton X-100, the cells were incubated for 1 h in blocking buffer that consisted of PBS and 10% normal goat serum, followed by an additional overnight incubation period with primary antibody (Table S2) in a humidified chamber at 4°C. The cells were subsequently incubated with the appropriate secondary antibody at room temperature for 45 min. For nucleus staining, we used 4,6-diamidino-2-phenylindole (DAPI; Sigma-Aldrich). Immunostaining without primary antibodies was used as the negative control for the cells.

Histological analysis

Teratomas in the teratoma assessment groups and ovarian tissue in the Sterilized mice were fixed in 10% formalin and 4% Bouin's solution. They were subsequently dehydrated in a graded ethanol series, vitrified in xylene, and embedded in paraffin and finally sectioned into 6 μm sections. These sections were mounted onto slides. The slides were de-waxed in xylene and rehydrated through an ethanol gradient and stained with hematoxylin and eosin (H&E, Sigma-Aldrich).

Detection of apoptosis by the TUNEL assay

We used the TUNEL assay to evaluate cell apoptosis in the aggregates. The aggreagte sections were each washed twice in PBS for 5 min after deparaffinization. The sections were permeabilized by incubation in 0.1% Triton X-100 and 0.1% sodium citrate for 8 min at room temperature. The sections were washed twice with PBS and incubated with the TUNEL reaction mixture (5 μl enzyme solution and 45 μl labeling solution) for 60 min at 37ºC in the dark. The negative control consisted of tissue sections

incubated with only labeling solution. After incubation with the reaction mixture, the sections were washed three times with PBS. Apoptotic cells (green fluorescence) were visualized by a fluorescence microscope (Olympus). Counterstaining with DAPI was used to visualize the nuclei.

This assay was performed using the Death Detection Kit (Roche Molecular Biology, Germany), which identifies apoptotic fragmented DNA by terminal deoxynucleotidyl transferase (TdT)-mediated incorporation of fluorescein-12-dUTP into the 30-hydroxyl end of DNA TdT.

Teratoma formation

We subcutaneously injected 1 x 10^5 ASCs into the neck area of three nude female mice (Pasteur Institute, Tehran, Iran). Controls were age-matched female nude mice that were injected at the same site with mouse ESCs (mESCs). The mice were monitored weekly for teratoma formation for up to three months.

Sterilization of adult mouse ovaries by chemotherapy

We intraperitoneally injected busulfan (30 mg/kg, resuspended in DMSO) and cyclophosphamide (120 mg/kg) into 2-month-old C57BL/6 female wild-type mice (28) (n=10). Controls were injected with DMSO. The transplantation of ovarian cells was performed one week after chemotherapy treatment and assessments were done 4 weeks after cell transplantation.

Sample preparation for RNA sequencing analysis

To assess gene expression profiles throughout the course of aggregate cell derivation, we initially collected samples from aggregates, ASCs at different time points (primary culture: P0, 4, 10, and 40) and MEFs (at least three biological replicates in each group). These time points were chosen to evaluate changes in transcriptions that occurred during derivation of the aggregate cells and their long-term culture. Due to the presence of MEF cells with different densities during the culture of the aggregate-derived cells, we chose the MEF samples for this cell contamination. The cells were collected and preserved at -80°C until RNA extraction.

Analysis of RNA-sequencing data

Initially all reads were controlled by FastQC (version 0.11.7)(29) followed by Trimmomatic (version 0.38) (30) for trimming low quality bases. The remaining reads were aligned to the mouse reference genome GRCm38 (downloaded from Ensembl database) (31) using HISATt2 (32). In order to find the differentially expressed genes (DEGs), we used the HTSeq (version 0.9.1)(33) and DESeq2(34) packages and the R program for finding clusters using the K-means algorithm. We performed gene ontology (GO) analysis using the Enrichr (35) package in the R program for both enriched GOs and biological pathways.

Heat map clustering, volcano plot, principal component analysis (PCA), and K-means clustering were performed using the R studio platform. GO and functional enrichment were assessed with Enrichr (https://amp.pharm.mssm.edu/Enrichr/) by taking into consideration enriched functions in at least two

different data bases (Kyoto Encyclopedia of Genes and Genomes [KEGG] 2016, Wiki Pathways 2016, Biocarta 2016, and Reactome Pathway 2016 as well as GO terms 2018).

Small molecule treatment

We plated 200.000 aggregate-derived cells that were cultured for at least 40 passages onto 12-well plates with basal culture medium or basal medium supplemented with 10 ng/ml IL-6 (36), different concentrations of JAK inhibitor and Stat3 inhibitor or basal medium without LIF. Three replicates for each condition were examined. Cell number and viability were counted after three days using a hemocytometer after trypan blue staining.

Image analysis and cell counts

We determined the numbers of ASCs, OLCs, and Ki67-positive cells with wide angle (20x) images that covered approximately 200–1000 cells per image in ImageJ software using the 'cell counter' plugin. We counted at least five fields of view for every condition.

Statistical analysis

All experiments were conducted in at least three independent replications. All data are expressed as mean ± SD, and analyzed by student's *t*-test. All graphs were generated using GraphPad Prism software version 8.0. P-values <0.05 were considered significant.

Data availability

The datasets and computer code produced in this study are available in the following database:

RNA-Seq data: Gene Expression Omnibus (GEO) under accession number the submission ID= PRJNA664684.

Results

Ovarian aggregate formation

We initially developed ovarian aggregates in a 3D culture system by preparing 3×10^5 mouse single ovarian cells per 3 cm^2 plate (Fig. 1Aa). These cells generated aggregates (50-100 μm diameter) within 2–3 days after cell seeding on the agarose-coated plates (Fig. 1Ab-d). We determined the localization of the cells by immunostaining. The aggregates exhibited an outer rim that expressed the Extracellular Matrix (ECM) markers laminin (37) and fibronectin (38) (Fig. 1B). Some of the cells in the aggregates expressed the stromal marker AMH (39) (Fig. 1B). The internal cells expressed germ cell markers that included Dazl and Ddx4(40) (Fig. 1B). A few intermediate cells expressed both germline and stromal markers. Ddx4/Ki67 double-positive cells in the aggregate showed the presence of germ cell-like cells with proliferating activity (Fig. 1B). Hormone analysis in the aggregate showed secretion of β-estradiol

(E2) and inhibin in response to gonadotropins (FSH and LH)(41) (Fig. 1C). The TUNEL assay results indicated that the viability rate of these aggregates was approximately double compared to ovarian cells grown in the 2D culture (Fig. 1D, E). Collectively, these observations demonstrated that the 3D culture of adult mouse ovarian cells could support the formation of aggregates.

Derivation and expansion of aggregate-derived stem cells

We plated five aggregates in 0.5 ml of medium per well of a 12-well plate that was coated with inactivated mouse embryonic fibroblasts (MEFs). After three days, we observed round cells that were approximately 10 µm in size that emerged around the aggregates (Fig. 2A). These cells increased in number and some formed grape-like clusters. These cells became confluent after three weeks and we passaged them by 0.05% trypsin-EDTA at a 1:2 split ratio (Fig. 2A).

Cells that emerged from the aggregates expressed markers have been known as germ line stem cells markers(40) *Prdm1*, *Dppa3*, *Ifitm3*, *Ddx4*, *Dazl*, *Oct4* and pluripotency markers *Oct4* and *TERT* (42, 43) (Fig. 2B). Immunofluorescence analysis also confirmed expressions of Ddx4, Dazl, Dppa3, Oct4, Prdm1, and Ifitm3 markers at the protein level (Fig. 2C). But the aggregated-emerged cells were negative for thecal stem cell markers(44, 45) CD29, CD90, and Lhr (Supplementary Fig. 3). We examined these cells by dual immunofluorescence staining for Ddx4 and Ki67 to test whether they expressed germ cell markers with proliferating activity. The results indicated that most Ddx4-positive cells expressed Ki67 (Fig. 2D). These results confirmed that the cells which proliferated and emerged from ovarian aggregates were mitotically active cells that expressed germ cell markers. Hereafter, we called them aggregated-derived stem cells (ASCs).

Next, we assessed the ability of ASCs to expand *in vitro*. They were passaged every three to four weeks in 0.05% trypsin-EDTA at a 1:2 split ratio and cultured on new MEF-coated plates (Fig. 3A). After P4-5, the ASCs proliferated more rapidly and needed to be passaged every four to five days with a split ratio of 1:3 (Fig. 3B). Of note, we could propagate them *in vitro* for 90 passages over a two-year period. Moreover, these expanded cells could be successfully freeze-thawed and underwent propagation *in vitro* after re-culturing with no significant differences in cell viability before and after the freeze-thawed process (Fig. 3C, D).

We observed co-expression for Ddx4 and Ki67 during the long-term culture of the ASCs (Fig. 3E-F) or after the freeze-thawed process (data not shown). In addition, these long-term cultured cells expressed Ddx4, Dazl, Dppa3, Oct4, Prdm1, and Ifitm3 after long term culture (P12) (Fig. 3G). These findings demonstrated that ASCs could undergo long-term propagation in culture and still maintain their primary culture characteristics.

The ASCs also expressed very low alkaline phosphatase (AP) as an indicator of pluripotent stem cells (Supplementary Fig. 4A) (42, 46). We examined the tumorigenicity of the *in vitro* cultured ASCs and found no evidence of tumor formation in nude female mice that were transplanted (n=3) with these ASCs, even at 12 weeks after transplantation (Supplementary Fig. 4B). However, control mice (n=3) that received the

mouse ESCs had evidence of teratoma formation in the neck region within four weeks (Supplementary Fig. 4B). These results demonstrated an intrinsic nature for ASCs, which somehow differed from pluripotent stem cells.

This approach was highly reproducible. We isolated ASCs 20 times from 20 biological replicates using eight adult mouse ovaries per replicate.

In vitro differentiation of oocyte-like cells from mouse ASCs

During culture of ASCs, we observed the expression of large spherical cells of up to 55 µm in size spontaneously formed upon *in vitro* culture of ASCs (Fig. 4B). These large cells were morphologically similar to oocytes; therefore, we called them oocyte-like cells (OLCs) (Fig. 4B). Then, we tested whether directed differentiation could improve OLC formation and found that the media with oocyte maturation factors (Fig. 4A, Table S3) would produce OLCs up to 75 µm in diameter (Fig. 4Bc). There were more, larger-sized OLCs that underwent directed differentiation compared to the spontaneously formed OLCs (Fig. 4C, D).

The OLCs expressed oocyte-specific markers(40) *GDF9*, *Zp1*, *Sycp3*, *Nobox*, and *Lhx8* (Fig. 4E). Immunofluorescence analysis revealed that OLCs expressed Gdf9, Zp1, and Ddx4 at the protein level, which are specific to germ cells at the oocyte stage. The OLCs expressed c-Kit, which is routinely expressed in the cytoplasm of oocytes at all stages of follicle development (47)(Fig. 4F).

Taken together, we established a highly reproducible method for isolation of mitotically active germ cell-like cells that used an adult mouse aggregate approach.

In vivo evaluation of mouse ASCs

We sought to determine the function of the ASCs by injecting them (1×10^4 cells/ovary) into the ovaries of female mice one week after the animals underwent chemotherapy treatment with cyclophosphamide (120 mg/kg body weight) and busulfan (30 mg/kg body weight). We found numerous remnants of degenerated follicles in the ovaries of the sterilized vehicle recipients (n=5), (Fig. 5A). However, in ASCs injected mice (n=5), the ovaries became more structured and new primordial and primary follicular structures formed in the ovaries four weeks after cell transplantation. (Fig. 5B).

Establishment of aggregates from adult human ovarian samples

We applied the same procedure as mouse ASCs for isolation and seeding eight ovarian samples (35–45 years of age) (Supplementary Fig. 1). Initially, we generated human aggregates according to the same protocol for mouse aggregates. We observed the appearance of follicle-like structures in the human aggregates (Fig. 6Aa-d). The outer rim of human aggregates, like mouse aggregates, expressed laminin and fibronectin and some cells expressed AMH. The inner localized germ cells were characterized by expressions of DDX4 and DAZL (Fig. 6B). Human aggregates immunostained for Ki67 and DDX4

demonstrated proliferative Ki67-positive cells that expressed DDX4 dispersed along the aggregates (Fig. 6B).

We investigated the capacity of human aggregates to support ASCs generation. The aggregates were replated on inactivated MEF-coated plates according to the procedure for mouse aggregates. The human ASCs were expanded *in vitro* for 240 days (Fig. 7A-B). The proliferation rate of human ASCs was lower than mouse ASCs, which were passaged every 30 days with a split ratio of 1:2. The expanded human ASCs concurrently expressed Ki67 and DDX4, which provided evidence of their proliferative capacity (Fig. 7C, D). The ASCs expressed DDX4, DAZL, DPPA3, OCT4, PRDM1, and IFITM3 (Fig. 7E). This approach was reproducible, as we isolated ASCs eight times from eight patients. However, the isolated ASCs could only be passaged for 3-8 passages in 3 cases. Moreover, human ASCs spontaneously differentiated into 80-100 μm diameter OLCs that expressed the oocyte-specific markers GDF-9 and ZP1 (Fig. 8A, B).

Therefore, we showed that adult human aggregates supported the efficient isolation of ASCs with the expressions of markers, and potential for self-renewal and differentiation into OLCs *in vitro*

Transcriptome analysis for mouse ASCs

Transcriptional profiling of their mRNA with RNA-sequencing (RNA-seq) in different passages of ASCs was performed and compared with aggregate and MEF. We used clustering and principal component analysis (PCA) to determine the relationships between groups, which also revealed reproducibility in the transcriptome data. Hierarchical clustering showed major clusters of aggregates, ASCs at different passages (P0, 4, 10, and 40), and MEF (Fig. 9A). Dimension reduction of gene expression data by PCA depicted a striking similarity between ASCs in different passages (P4, 10, and 40) that were clustered together and apart from aggregates and ASCs at P0 (Fig. 9C). The close relationship between ASCs-P0 and MEF cells (Fig. 9C) might reflect residual MEF contamination, which was higher at P0 than the other passages. The same clustering of passaging cells (Fig. 9A,B) demonstrated that these cells maintained their characteristics even after extended passaging. A volcano plot (Fig. 9B) was employed to identify the top differentially expressed genes (DEGs). There were 892 genes that upregulated in the first passage of ASCs compared to the aggregates and 2343 genes that upregulated in further passages (P4, 10, and 40) compared to ASCs-P0 (Fig. 9B). Extracellular matrix organization and glutathione metabolic processes (GO biological process terms) were enriched in aggregates and ASCs-P0, respectively (Fig. 9B left panel), while cytokine receptor activity term was downregulated by passaging the ASCs (Fig. 9B right panel).

A K-means (K=8) clustering analysis was subsequently conducted to group genes with similar behaviors. The profile plots for each cluster with the thick red lines representing the learned cluster center is shown in the Figure 9D. Genes in clusters 5 and 2 exhibited increased expression in P0 and aggregates respectively, decreased in subsequent passages and then remained unchanged. Enriched functions in cluster 2 encompassed epithelium development and vasculogenesis and in cluster 5 is extracellular matrix organization. Clusters 3 and 4 respectively contained 587 and 1270 genes, whose expression

increased in P0 and remained unchanged during subsequent passages. These clusters were enriched in neutrophil mediated immunity and degranulation.

We also performed a gene ontology (GO) analysis based on the genes that were upregulated in ASCs during different passages (P0, 10, and 40). Intriguingly, we observed that the germ cell markers such as, *Ddx4*, *Dppa3*, *Dazl*, and *Oct4* were poorly represented in the transcriptome of the ASCs in P0 and higher passages, however *Prdm1*, *Cpeb1* and *Ifitm3* is found in cluesters 3 and 4 (Fig. 9D).

The role of JAK/STAT3 signaling pathway for maintaining self-renewal in ASCs

The DEG enriched pathways according to KEGG analysis of the ASCs revealed an upregulation of pathways related to the inflammatory response and neutrophil function in these clusters (Supplementary. Table S4). This was particularly remarkable for signaling pathways related to interleukin 6 (IL-6) in cluster VIII (Table S4). It has been shown that IL-6 activates the Janus kinases (JAKs)/signal transducer and activator of transcription proteins (JAK/STAT3) pathway and enhances cellular proliferation and stemness(48, 49). These findings raised the question of whether IL-6 and the JAK/STAT3 signaling pathway would be one of the principal active pathways during the passaging of ASCs. Moreover, we used LIF in our culture medium, which also activates JAK/STAT3 signaling(50, 51). In order to examine the function of this pathway in the maintenance and proliferation of ASCs, we assessed cell counts and viability after adding IL-6 to our culture media, removing LIF, and inhibiting JAK and STAT3 by small molecules, 420099 and Stattic, respectively (Fig. 10A). We examined selected concentrations of inhibitors, JAK inhibitor (0.6, 1.2, 1.8, 2.4 μM) and Stat3 inhibitor (0.5, 1, 2, 5, 10 μM)] (36, 52-55) (Supplementary Fig. 4). The cells were maintained and proliferated with or without IL-6 with no considerable changes in morphology, viability or cell numbers (Fig. 10B-D). Following increasing the concentration of JAKi, the cell number dramatically decreased. We detected a significant decrease in cell numbers with morphological alterations including transition from rounded to spindle like cells compared to the control group in 2.4 μM concentration of JAKi, while the cell viability did not change (Fig. 10B-D, Supplementary Fig. 4). Of note, when LIF was depleted from the culture medium, we observed a remarkable decrease in cell numbers as well as morphological changes (Fig. 10B,C). Treating the cells with increasing concentrations of Stat3i, led to a decrease in cell numbers, while cell viability decreased significantly following treatment only with 10 μM of Stat3i (Supplementary Fig. 4). According to the morphologically changes, reduction in cell numbers and unaffected viability in the groups treated with 2 μM of Stat3i and 2.4 μM of JAKi (Fig. 10B-D), we propose that JAK/STAT3 signaling pathway contributed to ASCs proliferation.

Discussion

Our study reports an *in vitro* platform for aggregate formation from ovarian tissue that enables a highly reproducible system for efficient derivation of proliferating stem cells. We provided an aggregate system from whole ovarian cells (without mature oocyte) to make communication between germ cells and somatic cells that is critical for stem cell maintenance and germ cell proliferation(56). Here, we used from

mouse and human whole ovarian cells (without mature oocyte) and three-dimensional (3D) culture approach to provided permissive and suitable niche for the survival and propagation of ASCs. The 3D aggregate cultures mimic physiological conditions *in vitro* by supporting intensive communication between cells, and provide biomechanical and biochemical cues that mediate intercellular functions(57). It is well known that bilateral connection between mature oocyte and ovarian somatic cells is require for meiotic arrest of mammalian oocyte (58–60), so depletion of mature oocytes in our aggregate system removed this inhibitory effect, and provided a suitable niche for the survival and proliferation of the ASCs.

Live and dead cell analyses confirmed that the aggregates exhibited much higher ovarian cell viability compared with the 2D culture. Our results were consistent with previous findings, which showed that cell viability, proliferation, gene and protein expressions, stable morphology, and general cell function were more consistent in the 3D culture compared to 2D cultures(20). We found that our aggregates secreted E2 and inhibin in response to LH and FSH, as does the ovary(61). In addition, we demonstrated that these aggregates efficiently expressed a proliferation marker (Ki67)(62, 63) and germ cell markers (Ddx4 and Dazl)(64). The double Ki67 and Ddx4 positive cells were also reported in the adult mouse ovarian surface epithelium(65). Of note, all Ddx4-positive cells did not express Ki67, which demonstrated the presence of a mitotically active germ cell population in both mouse and human aggregates. However, a limitation of this study is that specific markers for ovarian cells other than germ cells were not evaluated. Such data may give us a deeper view of ASCs. These mouse ASCs showed high potential for *in vitro* expansion; the isolated ASCs propagated for 90 passages for more than two years. We observed that ASCs spontaneously produced OLCs that had a similar morphology and gene expression profiles as mouse oocytes when cultured *in vitro*. OSCs isolated by DDX4 spontaneously produced 35–50 μm diameter OLCs(9). Here, we improved ASCs differentiation to OLCs by the addition of FSH, ITS, EGF and LH, which acts on oocyte development *in vitro*(56, 66). Directed differentiation produced more OLCs than spontaneous formation. *In vitro* maturation media support the culture of OLCs up to 75 μm in size, which characterizes oocytes at the antral follicle stage(67). Oocyte maturation is normally triggered by LH, EGF, ITS, and FSH. These hormones, in turn, would cause cytoplasmic maturation of the oocytes(68, 69).

Hierarchical clustering of their transcriptomes demonstrated more similarities between P10 and P40 cells than with the P4 cells. This finding was consistent with the morphological observations, so that the growth of ASCs during the initial culture phases was very slow, after five passages, we observed a dramatic increase in cell growth rates that reflected the transitional stage from P4 cells to higher passages.

Our data obtained from RNA-sequencing revealed that the most upregulated genes in ASCs at various passages were associated with immune cells and an inflammatory response. Regarding this finding, it is notable that these cells were immune-positive for germ line markers but did not show upregulation expression in RNA-sequencing data. These results were in accordance with a recent report that identified a complete map of cell types in the human ovarian cortex by single-cell analysis(70). Wanger et al. found the cells that were sorted based on expression of DDX4 and were immune-positive for DDX4 antibody while not expressing DDX4 transcript(70).

RNA Seq analysis highlighted immune system-related pathways including inflammatory response with especially on the IL-6-mediated signaling pathway in ASCs. An increasing number of studies indicate that correlation between the IL-6 and activation of JAK/Stat3 signaling pathway for maintaining self-renewal in the stem cells(51, 71, 72). The important role of JAK/Stat3 signaling pathway in this study was confirmed by the use of small molecules that inhibit this pathway and by removal of LIF as the main activator factor for this signaling pathway. Our finding is in line with a recently published study that showed activation of immune system related pathways including inflammatory response and STAT pathways contribute to stemness in ovary surface epithelium(73). Moreover, the critical role for LIF in maintaining self-renewal and pluripotency of mouse embryonic stem cells (mESCs)(74, 75) were confirmed in previous reports and our findings are in line with previous studies (76–78). The role of the JAK/STAT3 signaling pathway in numerous developmental and homeostatic processes that include hematopoiesis, immune cell development, stem cell maintenance, organismal growth, and mammary gland development are well known(79).

The insight and model explained here is valuable for better understanding of ovarian stem cells and their using to clinical applications. According to the best of our knowledge, this report is the first to demonstrate the role of JAK/STAT3 pathway on proliferation of ASCs. Future lineage-tracing studies is necessary to elucidate the role of ovarian stem cells in homeostasis, tissue injury and reproductive tract.

Declarations

Acknowledgment

We are grateful to Dr Saadi Khochbin and Dr Sophie Rousseaux for help with the bio-informatics analyses and Pouya Tavakol for his kind contribution to the transplantation of ASCs into mouse ovaries.

Author contributions

M.S., and F.E., designed the experiments and analyzed the data. M.S., conducted the experiments. A. M. provided human ovarian tissue. M. S and F.E., wrote the manuscript. F.S., and A.M., did the bio-informatics analysis. M.M., helped for molecular analysis. F.E., supervised the research and took part in revising the manuscript. All the authors reviewed and approved the final manuscript for submission.

Funding

This work was supported by a grant from Royan Institute (No: 91000177) and the National Institute for Medical Research Development (NIMAD, grant no. 958379).

Ethical approval documentation

Ethics approval This study and all Human and animal experiments were approved by the Institutional Review Board and Ethical Committee of Royan Institute (Tehran, Iran). (No: Ec/92/1026)

The authors report no financial or commercial conflicts of interest.

Competing financial interests

The authors declare no competing financial interests.

References

1. Birbrair A. Stem Cells Heterogeneity. Adv Exp Med Biol. 2019;1123:1–3.
2. Bhartiya D, Ali Mohammad S, Guha A, Singh P, Sharma D, Kaushik A. Evolving Definition of Adult Stem/Progenitor Cells. Stem Cell Rev Rep. 2019;15(3):456–8.
3. Wang Y, Sacchetti A, van Dijk MR, van der Zee M, van der Horst PH, Joosten R, et al. Identification of quiescent, stem-like cells in the distal female reproductive tract. PLoS One. 2012;7(7):e40691.
4. Maruyama T, Masuda H, Ono M, Kajitani T, Yoshimura Y. Human uterine stem/progenitor cells: their possible role in uterine physiology and pathology. Reproduction. 2010;140(1):11–22.
5. Hummitzsch K, Anderson RA, Wilhelm D, Wu J, Telfer EE, Russell DL, et al. Stem cells, progenitor cells, and lineage decisions in the ovary. Endocr Rev. 2015;36(1):65–91.
6. Ng A, Barker N. Ovary and fimbrial stem cells: biology, niche and cancer origins. Nat Rev Mol Cell Biol. 2015;16(10):625–38.
7. Bhartiya D, Shaikh A, Anand S, Patel H, Kapoor S, Sriraman K, et al. Endogenous, very small embryonic-like stem cells: critical review, therapeutic potential and a look ahead. Hum Reprod Update. 2016;23(1):41–76.
8. Ye H, Zheng T, Li W, Li X, Fu X, Huang Y, et al. Ovarian Stem Cell Nests in Reproduction and Ovarian Aging. Cell Physiol Biochem. 2017;43(5):1917–25.
9. White YA, Woods DC, Takai Y, Ishihara O, Seki H, Tilly JL. Oocyte formation by mitotically active germ cells purified from ovaries of reproductive-age women. Nature medicine. 2012;18(3):413–21.
10. Wu BC, Kao CT, Huang TH, Hung CJ, Shie MY, Chung HY. Effect of verapamil, a calcium channel blocker, on the odontogenic activity of human dental pulp cells cultured with silicate-based materials. J Endod. 2014;40(8):1105–11.
11. Lopez J, Valdez-Morales FJ, Benitez-Bribiesca L, Cerbon M, Carranca AG. Normal and cancer stem cells of the human female reproductive system. Reprod Biol Endocrinol. 2013;11:53.
12. Blau HM, Brazelton TR, Weimann JM. The evolving concept of a stem cell: entity or function? Cell. 2001;105(7):829–41.
13. Dontu G, Abdallah WM, Foley JM, Jackson KW, Clarke MF, Kawamura MJ, et al. In vitro propagation and transcriptional profiling of human mammary stem/progenitor cells. Genes Dev. 2003;17(10):1253–70.
14. Hu WY, Hu DP, Xie L, Birch LA, Prins GS. Isolation of Stem-like Cells from 3-Dimensional Spheroid Cultures. J Vis Exp. 2019(154).

15. Zarate-Garcia L, Lane SI, Merriman JA, Jones KT. FACS-sorted putative oogonial stem cells from the ovary are neither DDX4-positive nor germ cells. Scientific reports. 2016;6:27991.
16. Zhang H, Zheng W, Shen Y, Adhikari D, Ueno H, Liu K. Experimental evidence showing that no mitotically active female germline progenitors exist in postnatal mouse ovaries. Proceedings of the National Academy of Sciences of the United States of America. 2012;109(31):12580–5.
17. Chacón-Martínez CA, Koester J, Wickström SA. Signaling in the stem cell niche: regulating cell fate, function and plasticity. Development. 2018;145(15):dev165399.
18. Ohlstein B, Kai T, Decotto E, Spradling A. The stem cell niche: theme and variations. Current opinion in cell biology. 2004;16(6):693–9.
19. Suda T, Arai F, Shimmura S. Regulation of stem cells in the niche. Cornea. 2005;24(8):S12-S7.
20. Antoni D, Burckel H, Josset E, Noel G. Three-dimensional cell culture: a breakthrough in vivo. International journal of molecular sciences. 2015;16(3):5517–27.
21. Crowell PD, Giafaglione JM, Hashimoto T, Diaz JA, Goldstein AS. Evaluating the Differentiation Capacity of Mouse Prostate Epithelial Cells Using Organoid Culture. J Vis Exp. 2019(153).
22. Nagamatsu G, Shimamoto S, Hamazaki N, Nishimura Y, Hayashi K. Mechanical stress accompanied with nuclear rotation is involved in the dormant state of mouse oocytes. Science advances. 2019;5(6):eaav9960.
23. Neumuller RA, Knoblich JA. Dividing cellular asymmetry: asymmetric cell division and its implications for stem cells and cancer. Genes Dev. 2009;23(23):2675–99.
24. De Bari C, Pringle S, Pitzalis C, Dell'Accio F. The stem cell niche: a new target in medicine. Current Opinion in Orthopaedics. 2006;17(5):398–404.
25. Zhang Y, Wang D, Xu J, Wang Y, Ma F, Li Z, et al. Stat3 activation is critical for pluripotency maintenance. Journal of cellular physiology. 2019;234(2):1044–51.
26. Huselstein C, de Isla N, Kolopp-Sarda MN, Kerdjoudj H, Muller S, Stoltz JF. Influence of mechanical stress on cell viability. Biorheology. 2006;43(3–4):371–5.
27. Aslam I, Robins A, Dowell K, Fishel S. Isolation, purification and assessment of viability of spermatogenic cells from testicular biopsies of azoospermic men. Human reproduction. 1998;13(3):639–45.
28. Zou K, Yuan Z, Yang Z, Luo H, Sun K, Zhou L, et al. Production of offspring from a germline stem cell line derived from neonatal ovaries. Nature cell biology. 2009;11(5):631–6.
29. Andrews S. FastQC: a quality control tool for high throughput sequence data. Babraham Bioinformatics, Babraham Institute, Cambridge, United Kingdom; 2010.
30. Bolger AM, Lohse M, Usadel B. Trimmomatic: a flexible trimmer for Illumina sequence data. Bioinformatics. 2014;30(15):2114–20.
31. Cunningham F, Achuthan P, Akanni W, Allen J, Amode MR, Armean IM, et al. Ensembl 2019. Nucleic acids research. 2019;47(D1):D745-D51.

32. Kim D, Paggi JM, Park C, Bennett C, Salzberg SL. Graph-based genome alignment and genotyping with HISAT2 and HISAT-genotype. Nature biotechnology. 2019;37(8):907–15.
33. Anders S, Pyl PT, Huber W. HTSeq—a Python framework to work with high-throughput sequencing data. Bioinformatics. 2015;31(2):166–9.
34. Love MI, Huber W, Anders S. Moderated estimation of fold change and dispersion for RNA-seq data with DESeq2. Genome biology. 2014;15(12):550.
35. Chen EY, Tan CM, Kou Y, Duan Q, Wang Z, Meirelles GV, et al. Enrichr: interactive and collaborative HTML5 gene list enrichment analysis tool. BMC bioinformatics. 2013;14(1):128.
36. Handle F, Puhr M, Schaefer G, Lorito N, Hoefer J, Gruber M, et al. The STAT3 inhibitor galiellalactone reduces IL6-mediated AR activity in benign and malignant prostate models. Molecular cancer therapeutics. 2018;17(12):2722–31.
37. Ricciardelli C, Rodgers RJ. Extracellular matrix of ovarian tumors. Seminars in reproductive medicine. 2006;24(4):270–82.
38. Heeren AM, van Iperen L, Klootwijk DB, de Melo Bernardo A, Roost MS, Gomes Fernandes MM, et al. Development of the follicular basement membrane during human gametogenesis and early folliculogenesis. BMC developmental biology. 2015;15:4.
39. Rocha RM, Lima LF, Carvalho AA, Chaves RN, Bernuci MP, Rosa-e-Silva AC, et al. Immunolocalization of the Anti-Mullerian Hormone (AMH) in Caprine Follicles and the Effects of AMH on In Vitro Culture of Caprine Pre-antral Follicles Enclosed in Ovarian Tissue. Reproduction in domestic animals = Zuchthygiene. 2016;51(2):212–9.
40. White YA, Woods DC, Takai Y, Ishihara O, Seki H, Tilly JL. Oocyte formation by mitotically active germ cells purified from ovaries of reproductive-age women. Nature medicine. 2012;18(3):413–21.
41. Messinis IE. Ovarian feedback, mechanism of action and possible clinical implications. Human reproduction update. 2006;12(5):557–71.
42. Wang H, Jiang M, Bi H, Chen X, He L, Li X, et al. Conversion of female germline stem cells from neonatal and prepubertal mice into pluripotent stem cells. Journal of molecular cell biology. 2014;6(2):164–71.
43. Esteves CL, Sharma R, Dawson L, Taylor SE, Pearson G, Keen JA, et al. Expression of putative markers of pluripotency in equine embryonic and adult tissues. The Veterinary Journal. 2014;202(3):533–5.
44. Chen H, Xia K, Huang W, Li H, Wang C, Ma Y, et al. Autologous transplantation of thecal stem cells restores ovarian function in nonhuman primates. Cell discovery. 2021;7(1):1–16.
45. Dalman A, Totonchi M, Valojerdi MR. Establishment and characterization of human theca stem cells and their differentiation into theca progenitor cells. Journal of cellular biochemistry. 2018;119(12):9853–65.
46. Stefkova K, Prochazkova J, Pachernik J. Alkaline phosphatase in stem cells. Stem cells international. 2015;2015:628368.

47. Tuck AR, Robker RL, Norman RJ, Tilley WD, Hickey TE. Expression and localisation of c-kit and KITL in the adult human ovary. Journal of ovarian research. 2015;8:31.
48. Shouda T, Hiraoka K, Komiya S, Hamada T, Zenmyo M, Iwasaki H, et al. Suppression of IL-6 production and proliferation by blocking STAT3 activation in malignant soft tissue tumor cells. Cancer letters. 2006;231(2):176–84.
49. Wang S-W, Sun Y-M. The IL-6/JAK/STAT3 pathway: potential therapeutic strategies in treating colorectal cancer. International journal of oncology. 2014;44(4):1032–40.
50. Niwa H, Ogawa K, Shimosato D, Adachi K. A parallel circuit of LIF signalling pathways maintains pluripotency of mouse ES cells. Nature. 2009;460(7251):118–22.
51. Onishi K, Zandstra PW. LIF signaling in stem cells and development. Development. 2015;142(13):2230–6.
52. Tesar PJ, Chenoweth JG, Brook FA, Davies TJ, Evans EP, Mack DL, et al. New cell lines from mouse epiblast share defining features with human embryonic stem cells. Nature. 2007;448(7150):196–9.
53. Alberio R, Croxall N, Allegrucci C. Pig epiblast stem cells depend on activin/nodal signaling for pluripotency and self-renewal. Stem cells and development. 2010;19(10):1627–36.
54. Schust J, Sperl B, Hollis A, Mayer TU, Berg T. Stattic: a small-molecule inhibitor of STAT3 activation and dimerization. Chemistry & biology. 2006;13(11):1235–42.
55. Pedranzini L, Dechow T, Berishaj M, Comenzo R, Zhou P, Azare J, et al. Pyridone 6, a pan-Janus–activated kinase inhibitor, induces growth inhibition of multiple myeloma cells. Cancer research. 2006;66(19):9714–21.
56. Bui HT, Van Thuan N, Kwon DN, Choi YJ, Kang MH, Han JW, et al. Identification and characterization of putative stem cells in the adult pig ovary. Development. 2014;141(11):2235–44.
57. Laschke MW, Menger MD. Life is 3D: Boosting Spheroid Function for Tissue Engineering. Trends in biotechnology. 2017;35(2):133–44.
58. McLaughlin EA, McIver SC. Awakening the oocyte: controlling primordial follicle development. Reproduction. 2009;137(1):1–11.
59. Telfer EE, Zelinski MB. Ovarian follicle culture: advances and challenges for human and nonhuman primates. Fertility and sterility. 2013;99(6):1523–33.
60. Wigglesworth K, Lee K-B, O'Brien MJ, Peng J, Matzuk MM, Eppig JJ. Bidirectional communication between oocytes and ovarian follicular somatic cells is required for meiotic arrest of mammalian oocytes. Proceedings of the National Academy of Sciences. 2013;110(39):E3723-E9.
61. Sittadjody S, Saul JM, Joo S, Yoo JJ, Atala A, Opara EC. Engineered multilayer ovarian tissue that secretes sex steroids and peptide hormones in response to gonadotropins. Biomaterials. 2013;34(10):2412–20.
62. Li LT, Jiang G, Chen Q, Zheng JN. Ki67 is a promising molecular target in the diagnosis of cancer. Molecular medicine reports. 2015;11(3):1566–72.

63. Jurikova M, Danihel Ľ, Polák Š, Varga I. Ki67, PCNA, and MCM proteins: Markers of proliferation in the diagnosis of breast cancer. Acta histochemica. 2016;118(5):544–52.
64. Bachvarova RF, Crother BI, Manova K, Chatfield J, Shoemaker CM, Crews DP, et al. Expression of Dazl and Vasa in turtle embryos and ovaries: evidence for inductive specification of germ cells. Evolution & development. 2009;11(5):525–34.
65. Johnson J, Canning J, Kaneko T, Pru JK, Tilly JL. Germline stem cells and follicular renewal in the postnatal mammalian ovary. Nature. 2004;428(6979):145–50.
66. Fortune JE. The early stages of follicular development: activation of primordial follicles and growth of preantral follicles. Animal reproduction science. 2003;78(3–4):135–63.
67. Griffin J, Emery BR, Huang I, Peterson CM, Carrell DT. Comparative analysis of follicle morphology and oocyte diameter in four mammalian species (mouse, hamster, pig, and human). Journal of experimental & clinical assisted reproduction. 2006;3:2.
68. Farin CE, Rodriguez KF, Alexander JE, Hockney JE, Herrick JR, Kennedy-Stoskopf S. The role of transcription in EGF- and FSH-mediated oocyte maturation in vitro. Animal reproduction science. 2007;98(1–2):97–112.
69. Morohaku K, Hirao Y, Obata Y. Developmental competence of oocytes grown in vitro: Has it peaked already? The Journal of reproduction and development. 2016;62(1):1–5.
70. Wagner M, Yoshihara M, Douagi I, Damdimopoulos A, Panula S, Petropoulos S, et al. Single-cell analysis of human ovarian cortex identifies distinct cell populations but no oogonial stem cells. Nature communications. 2020;11(1):1–15.
71. Kristensen DM, Kalisz M, Nielsen JH. Cytokine signalling in embryonic stem cells. Apmis. 2005;113(11-12):756–72.
72. Tang Y, Tian X. JAK-STAT3 and somatic cell reprogramming. Jak-Stat. 2013;2(4):e24935.
73. Carter LE, Cook DP, McCloskey CW, Grondin MA, Landry DA, Dang T, et al. Transcriptional heterogeneity of stemness phenotypes in the ovarian epithelium. Communications Biology. 2021;4(1):1–11.
74. Matsuda T, Nakamura T, Nakao K, Arai T, Katsuki M, Heike T, et al. STAT3 activation is sufficient to maintain an undifferentiated state of mouse embryonic stem cells. The EMBO journal. 1999;18(15):4261–9.
75. Niwa H, Burdon T, Chambers I, Smith A. Self-renewal of pluripotent embryonic stem cells is mediated via activation of STAT3. Genes & development. 1998;12(13):2048–60.
76. Huang G, Ye S, Zhou X, Liu D, Ying Q-L. Molecular basis of embryonic stem cell self-renewal: from signaling pathways to pluripotency network. Cellular and molecular life sciences. 2015;72(9):1741–57.
77. Davey RE, Onishi K, Mahdavi A, Zandstra PW. LIF-mediated control of embryonic stem cell self-renewal emerges due to an autoregulatory loop. The FASEB Journal. 2007;21(9):2020–32.

78. Zyuz'kov G, Udut E, Miroshnichenko L, Polyakova TY, Simanina E, Stavrova L, et al. Particular role of JAK/STAT3 signaling in functional control of mesenchymal progenitor cells. Bulletin of experimental biology and medicine. 2018;164(3):316–9.
79. Rawlings JS, Rosler KM, Harrison DA. The JAK/STAT signaling pathway. Journal of cell science. 2004;117(8):1281–3.

Figures

Figure 1

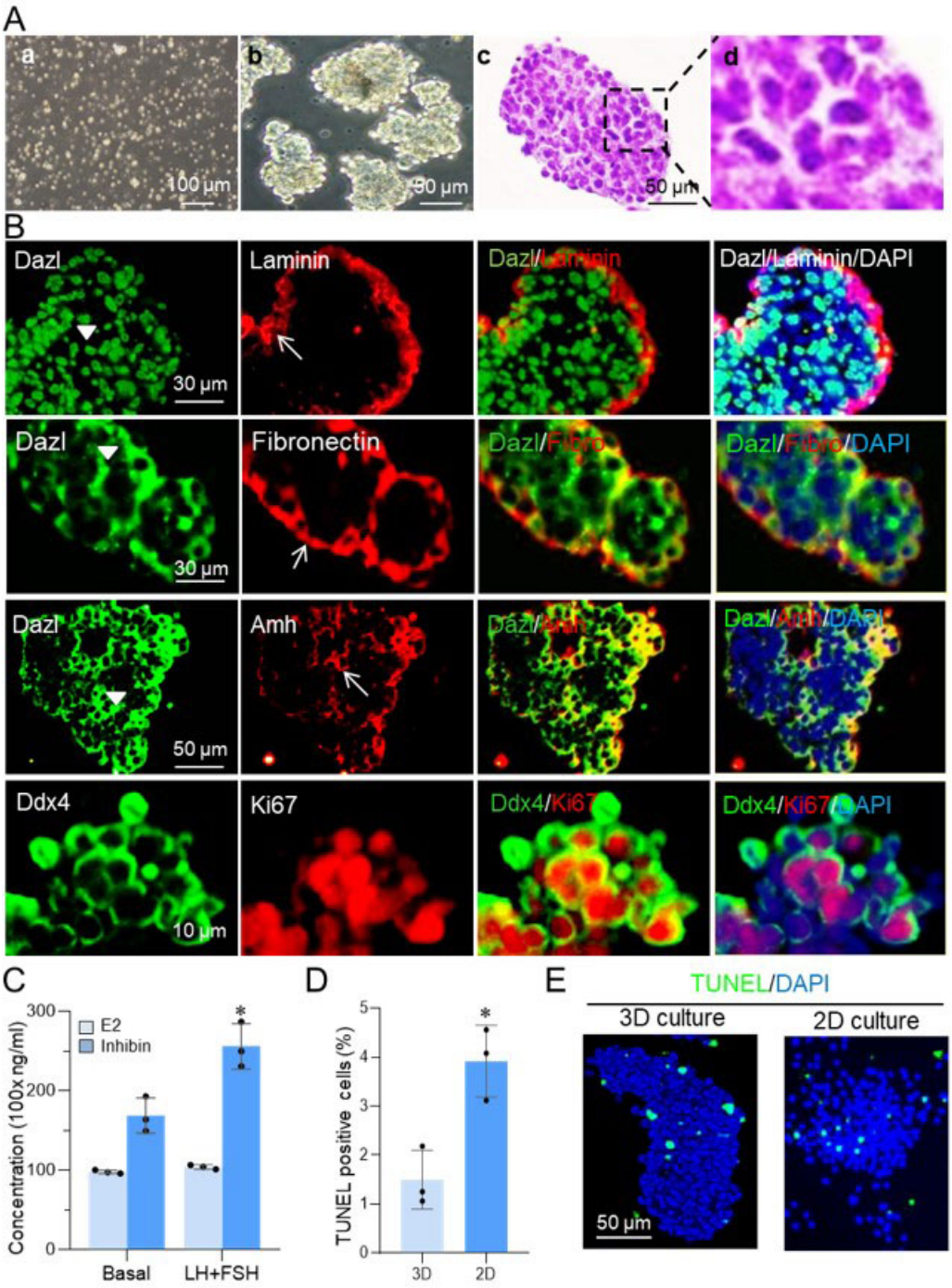

Figure 1

Mouse ovarian aggregates formation and characterization. (**A**) Phase-contrast images of mouse ovarian cell suspension after dissociation (a) and ovarian aggregates formation on day two (b). Histological image of two-day aggregates by hematoxylin and eosin (H&E) staining (c). Higher magnifications of the (c) panel indicate follicular-like structures (d). (**B**) Immunofluorescent images of aggregate sections show that aggregates contained cells that expressed Ddx4, Dazl (arrowheads), and AMH (arrows). Laminin and

fibronectin were detected in the outer rims of the aggregates (indicated with arrows). Many of the Ddx4-positive cells co-expressed the proliferation marker Ki67. Sections were counterstained with DAPI (blue) to visualize the nuclei. (**C**) β-estradiol (E2) and inhibin production by aggregates in the presence or absence of follicle stimulating hormone (FSH; 0.01 IU) and luteinizing hormone (LH; 7.5 IU) in basal medium (α-MEM medium with LIF, EGF, bFGF and GDNF). Data are presented as mean ± SD from three independent experiments (t-test, *P<0.05). **(D)** TUNEL assay for ovarian cells in a 2D compared with the 3D culture. **(E)** Quantification of the TUNEL assay. Error bars are the mean of at least five independent fields of view ± SD.

Figure 2

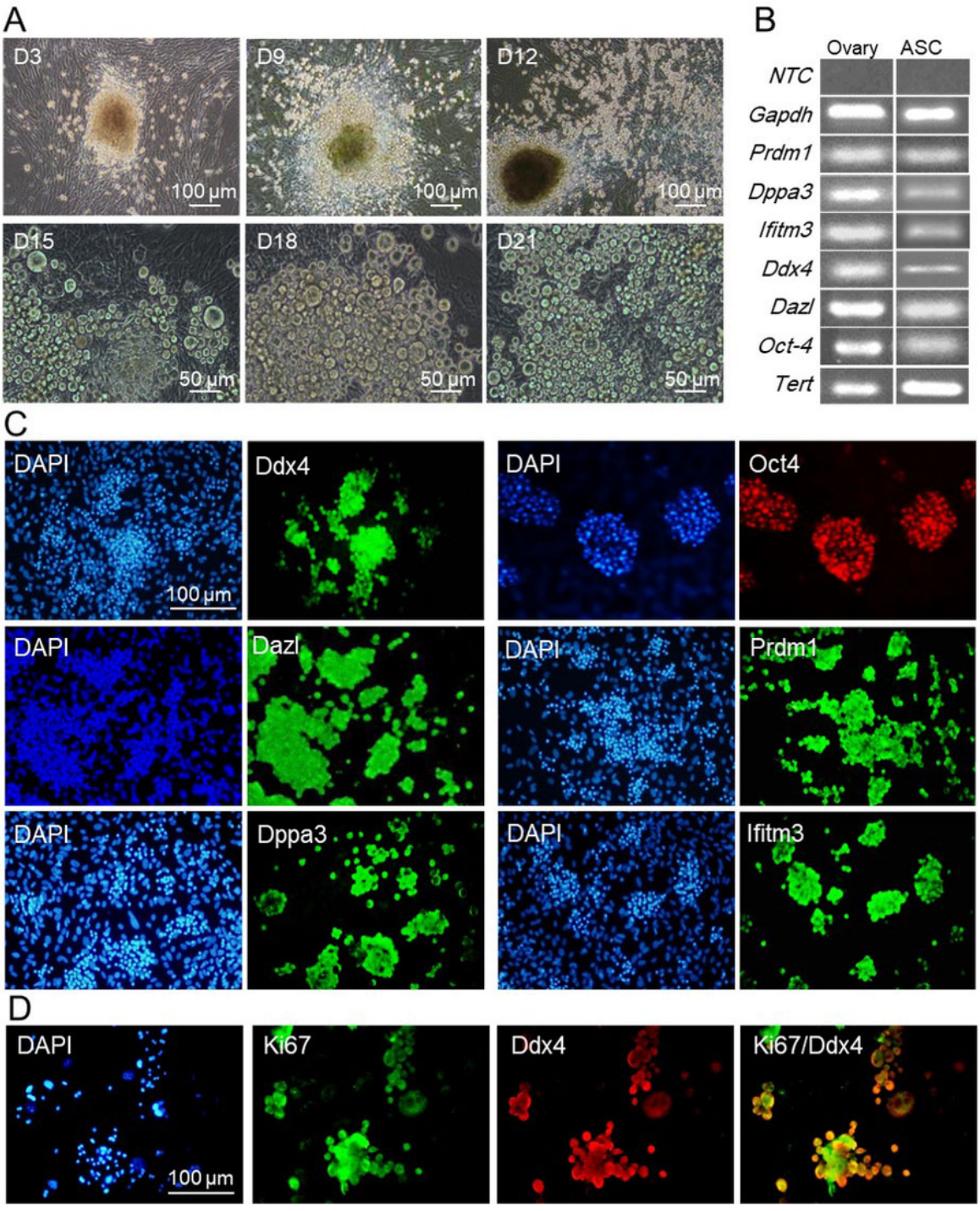

Figure 2

Characterization of ovarian aggregates-derived cells. (**A**) Phase-contrast images of plated aggregates and emergence of round cells on MEF. D: Day. (**B**) RT-PCR analysis of markers in aggregate-derived cells. An adult mouse ovary was used as the positive control. NTC refers to mock reverse-transcribed RNA samples. (**C**) Immunofluorescence staining of aggregate-derived cells for germ cell-specific markers. The feeder cells were negative for these markers. **(D)** Dual immunofluorescence staining of Ki67 (green) and

Ddx4 (red) expressions in aggregate-derived cells. Immunofluorescence staining for panels (C) and (D) were done two weeks after the aggregate plating.

Figure 3

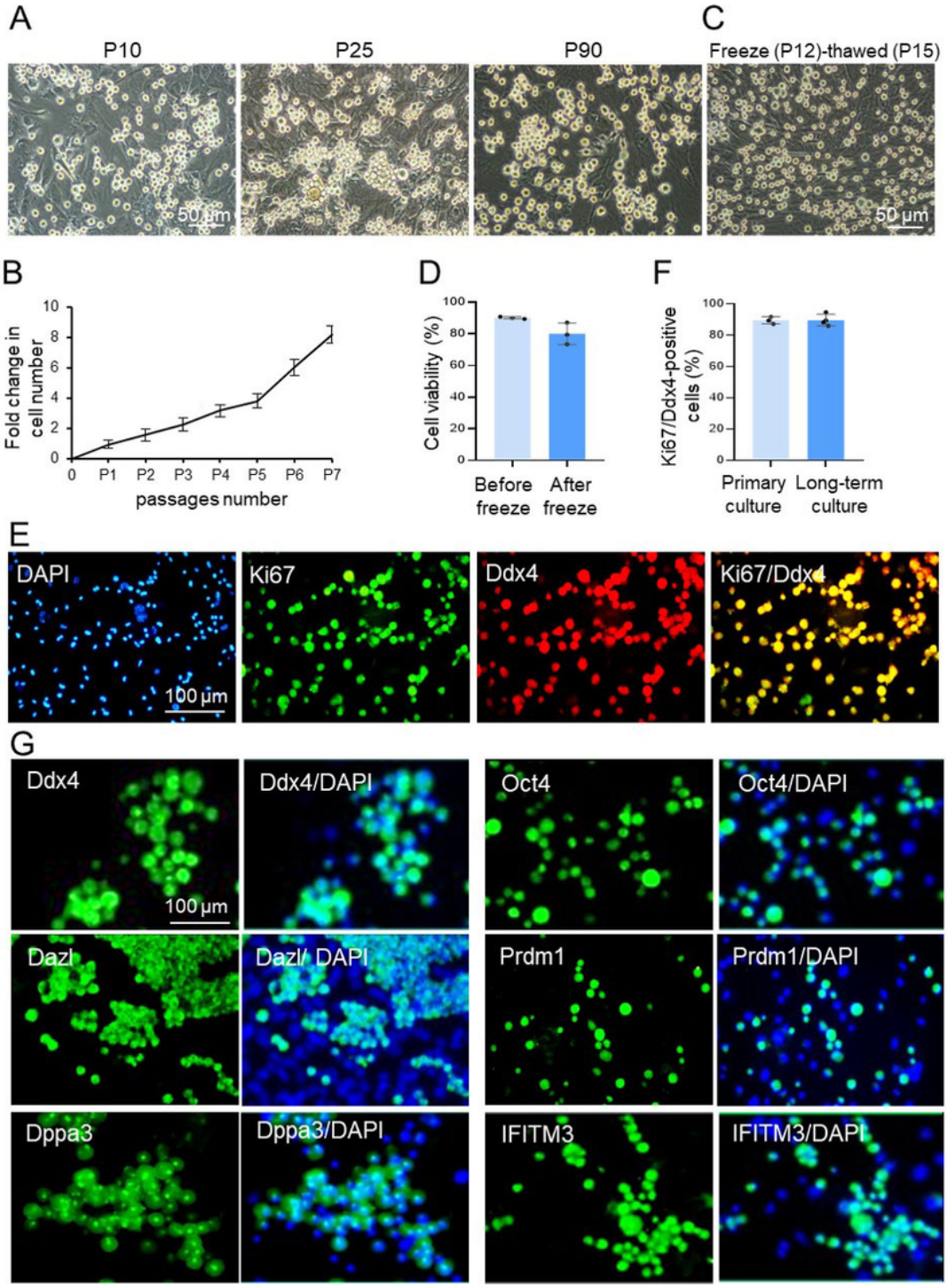

Figure 3

Characterization of long-term cultured mouse ASCs. (A) Phase-contrast images of expanded ASCs at different passages in culture on MEF-coated plates. (**B**) Long-term proliferation pattern of ASCs. (**C**) The

cells were frozen and propagated after thawing. **(D)** Cell viability before and after cryopreservation at P20. (**E**) Both Ki67 incorporation and Ddx4 expression were detected in the ASCs after long-term culture. (**F**) Quantification of ASCs (Ddx4-positive cells) and actively proliferating cells (Ki67-positive cells) in primary (day 21, before cell passage) and long-term (approximately five months, P12) cultures. Data are represented as mean ± SD for three independent experiments and analyzed by the t-test. (**G**) Immunofluorescence staining at P12. The feeder cells are negative for these markers.

Figure 4

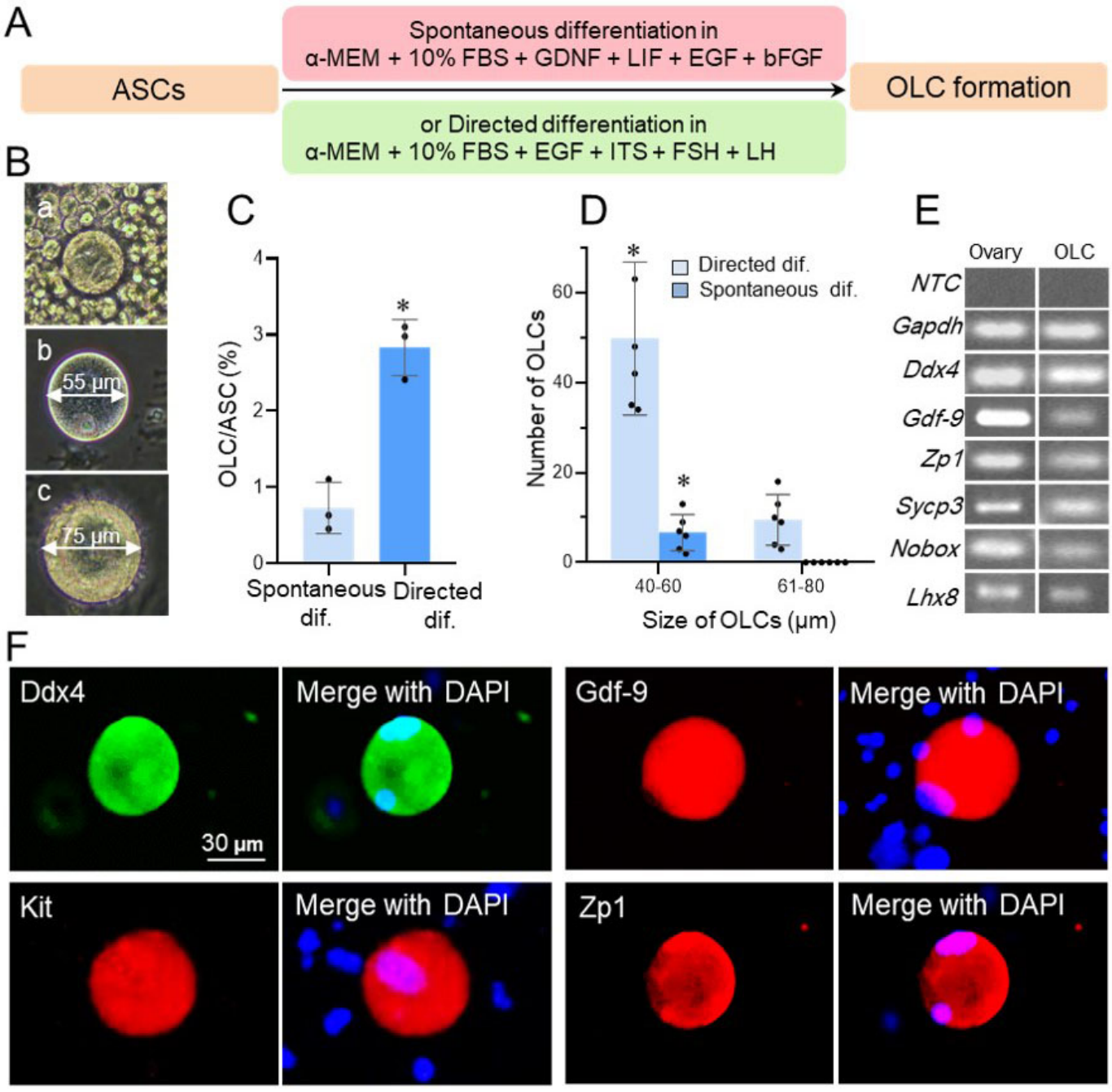

Figure 4

Characteristics of oocyte-like cells (OLCs) generated from mouse ASCs *in vitro*. **(A)** Schematic of the procedure for ASCs differentiation. (**B)** Phase-contrast images of formation of OLCs. (B-a) OLCs formation from ASCs. (B-b) Spontaneous generation of large spherical cells that morphologically resembled oocytes. (B-c) Directed differentiation media supported formation of OLCs that were up to 75 μm in diameter (**C, D**). Directed differentiation of ASCs to OLCs led to significantly larger and more

numerous OLCs in culture compared with spontaneously formed OLCs. Data represent mean ± SD for three independent experiments (t-test). Quantification of cell numbers using the ImageJ cell counter plugin. The images were captured with a wide angle (20x) and at least five fields were counted per condition. **(D)** Numbers of OLCs counted per five aggregates. **(E)** mRNA expression levels of oocyte-specific markers in spontaneously differentiated OLCs. (**F**) Immunofluorescence detection of germ cell and oocyte-specific markers in OLCs. Merged images of germ cell markers and DAPI in OLCs that were generated spontaneously from ASCs in MEF-coated plates.

Figure 5

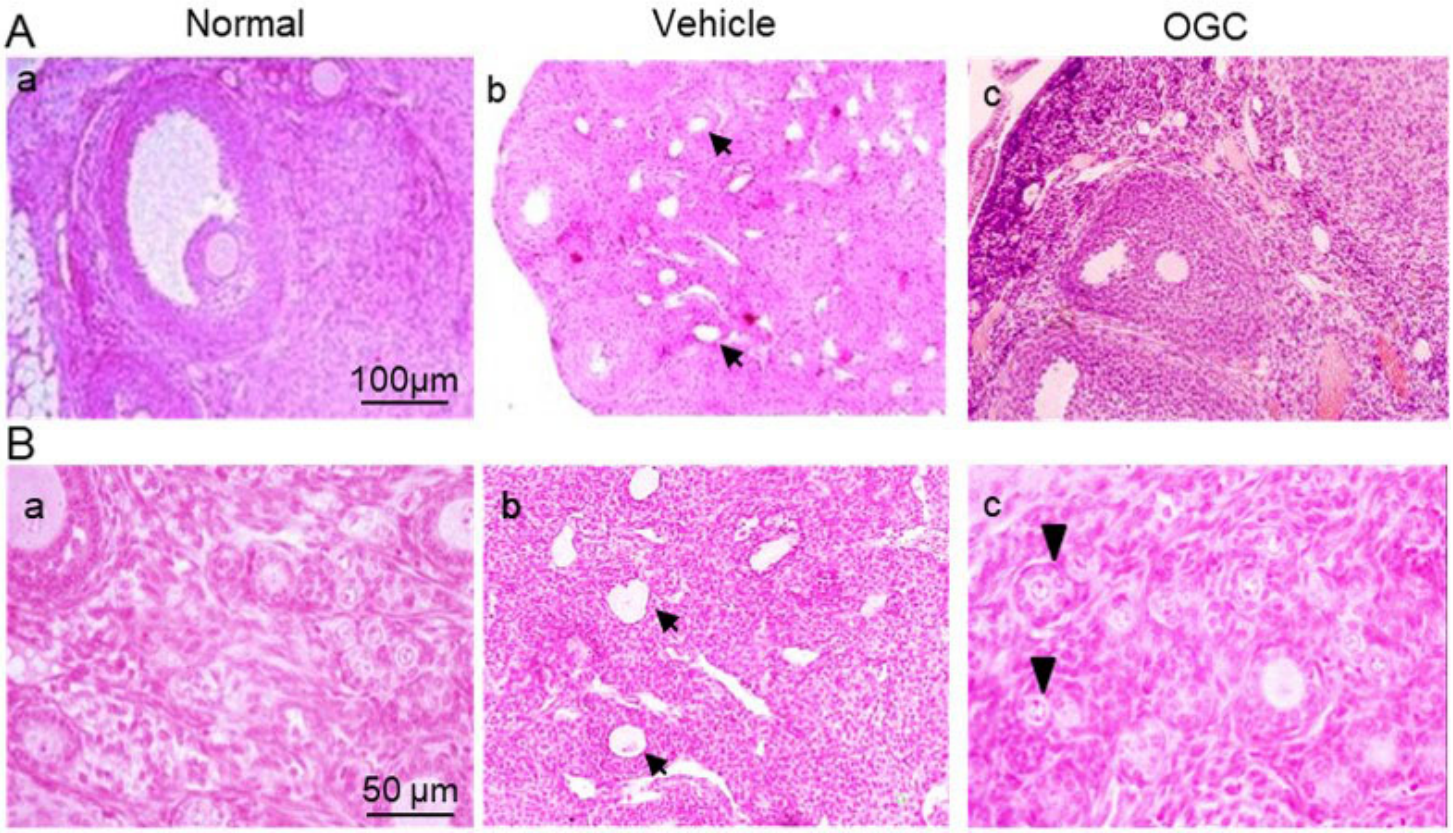

Figure 5

Transplantation of ASCs into mouse ovaries. (**A**) Hematoxylin and eosin (H&E) images. (A-a) The ovaries from control female mice (normal levels of follicle reserves), (A-b) sterilized recipient ovary (one week after chemotherapy treatment), the arrows indicate the presence of atretic primordial or primary follicles and (A-c) sterilized recipient ovary one month after ASCs injection. The arrowheads denote the new formed primordial and primary follicles. The mice were sterilized with intraperitoneal injection of cyclophosphamide and busulfan. (**B**) Higher magnifications of the panel (A).

Figure 6

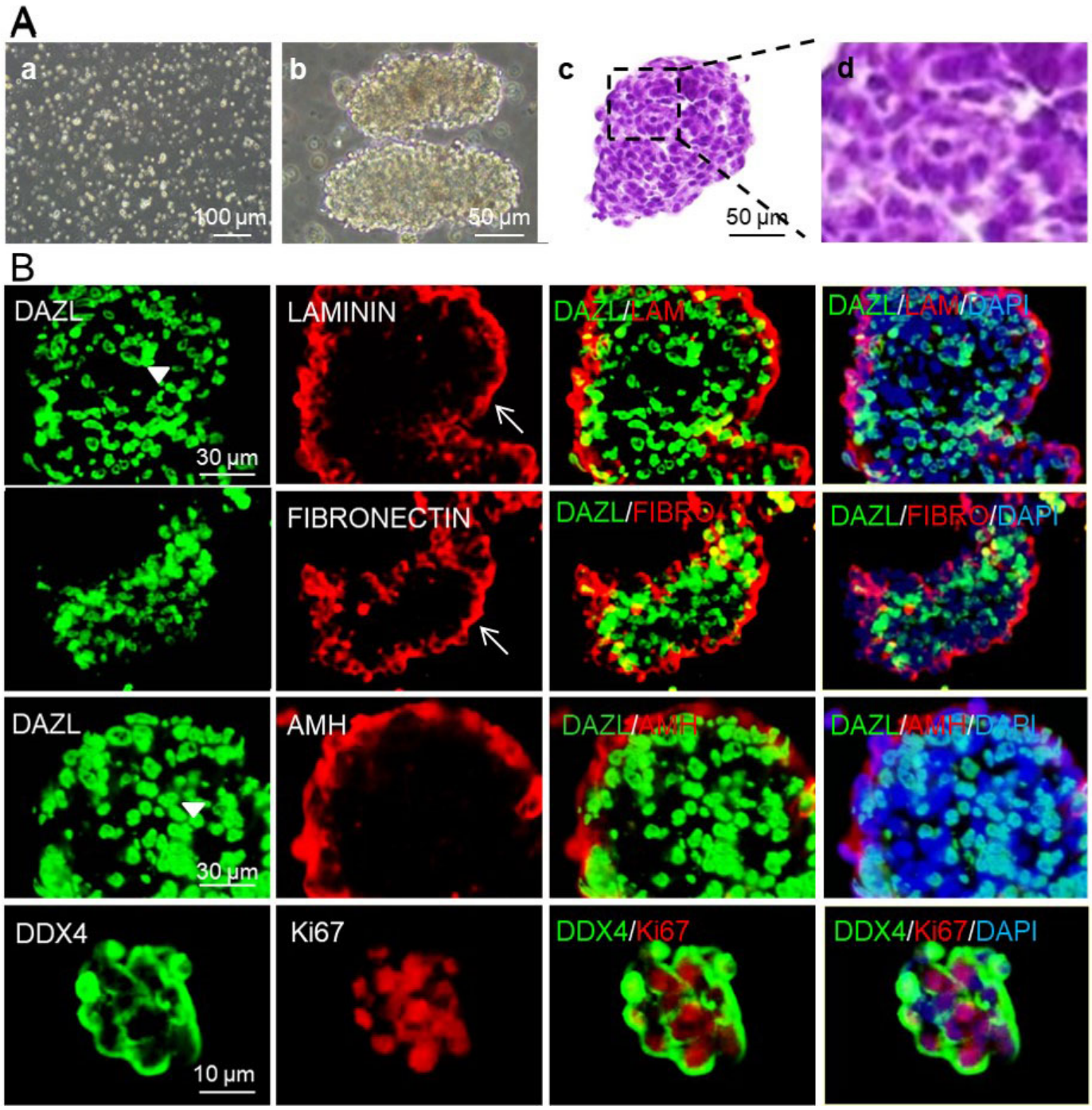

Figure 6

Establishment and characterization of human aggregates. (**A**) Phase-contrast images of human ovarian cell suspension after dissociation (a) and aggregate formation on day two (b). Histological image of aggregates according to H&E staining (c). The inset indicates the presence of follicular-like structures (d). (**B**) Immunofluorescent images of aggregate sections show that human aggregates contain laminin and fibronectin on the outer side (arrows) and the inner cells expressed germline markers, Ddx4 and DAZL

(arrowheads), and a stromal marker, AMH. Proliferating cells detected by immunofluorescence for Ki67. Germ cells with proliferating activity are shown by double immunostaining for Ki67 and Ddx4.

Figure 7

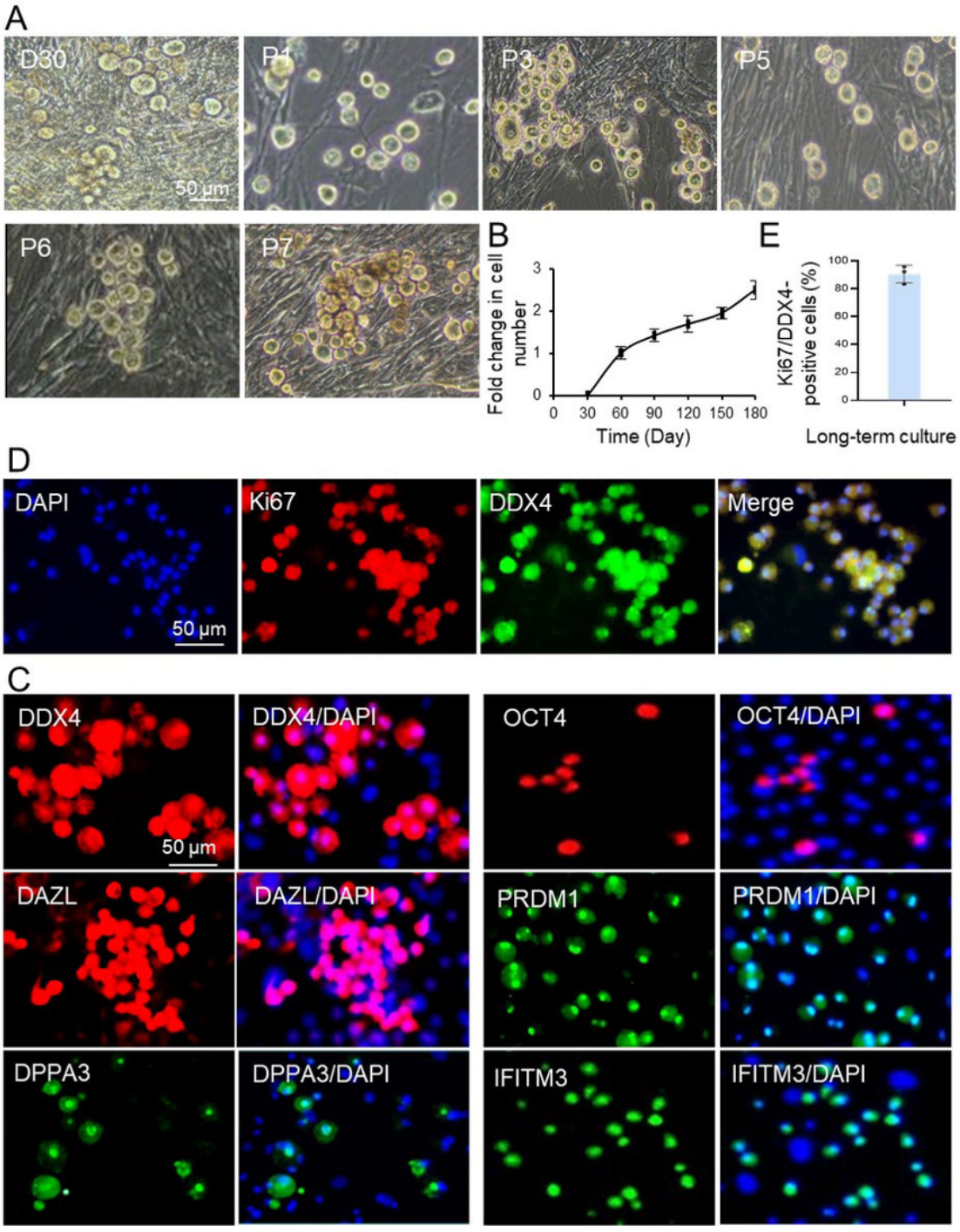

Figure 7

Emergence of ASCs after plating of human aggregates. (A) Phase-contrast microscope images of cultured cells during generation and passaging (day 30 in different passages: P1, P3, P5, P6, and P7) of ASCs on MEF-coated plates. (**B)** Growth curve of human ASCs. (**C**) Immunofluorescence staining for germline markers in human ASCs (after six passages) on MEF-coated plates. Cells were counterstained with 4,6-diamidino-2-phenylindole (DAPI, blue) to visualize the nucleus. **(D)** Immunofluorescence analysis for DDX4 and Ki67 in ASCs after six months in culture at P6. Nuclei were stained with DAPI (blue). (**E**) Quantification the number of Ki67/DDX4-positive cells over time (six months in culture). Data are mean ± SD from three independent fields of view.

Figure 8

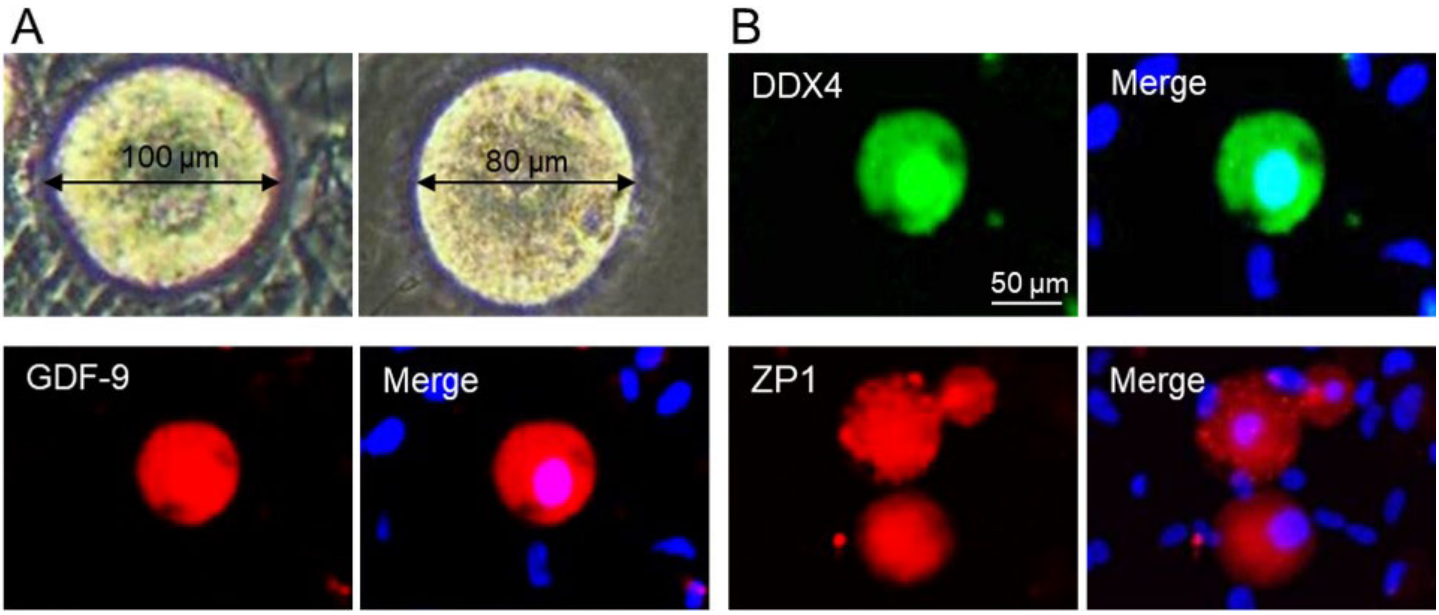

Figure 8

***In vitro* formation of oocyte-like cells (OLCs) from human ASCs. (A)** Morphological assessment of OLCs formed by human ASCs in culture (phase-contrast picture). (**B**) OLCs stained positive for DDX4, GDF9, and ZP1. The adjacent somatic cells were negative for these markers stained with DAPI.

Figure 9

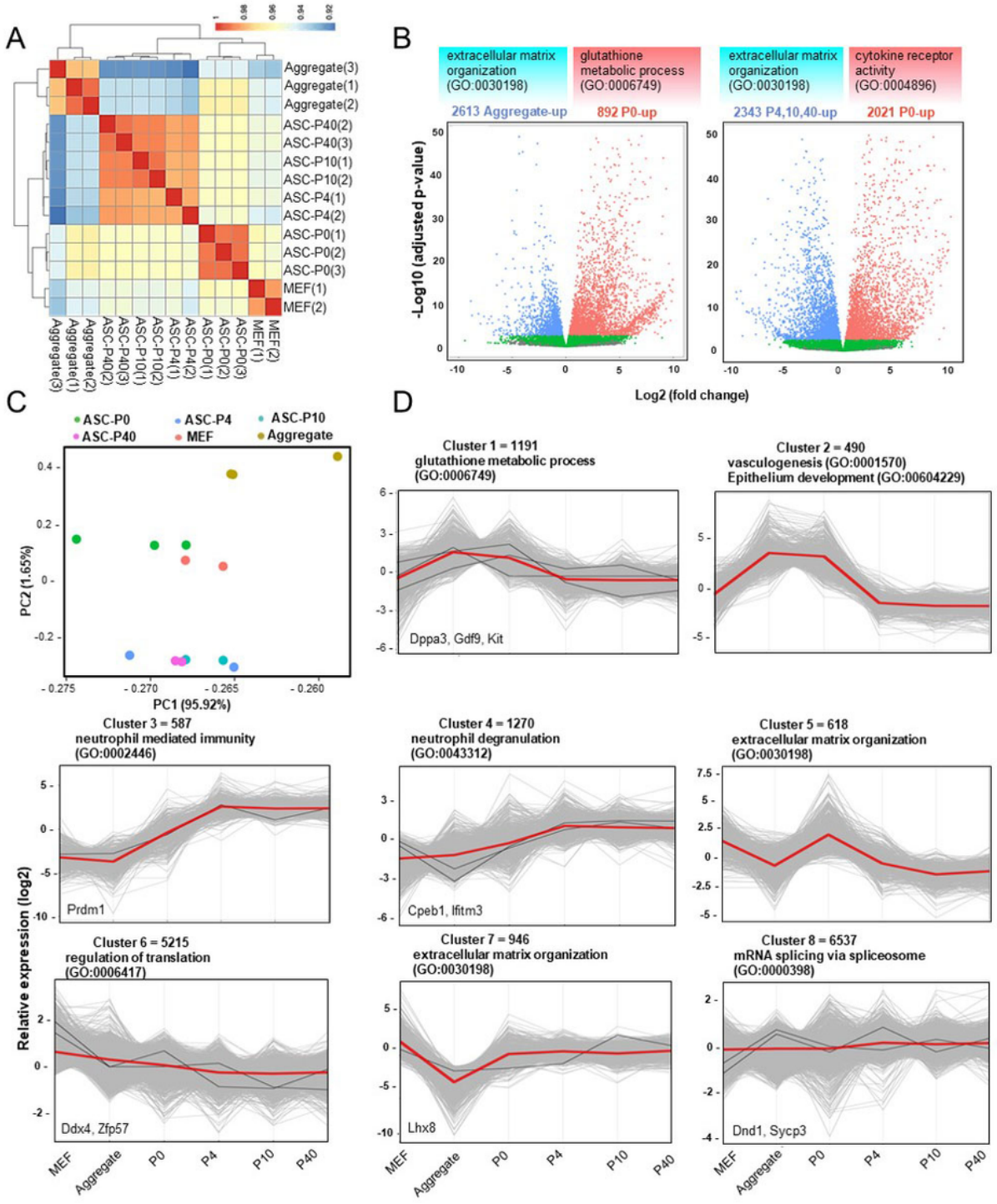

Figure 9

Transcriptome analysis. (**A**) Correlation heat map of gene expression data across cell types. The vertical distances on each branch of the dendrogram represent the degree of similarity between gene expression profiles of various samples. (**B**) Volcano plot to inspect ASCs between P0 and aggregate (left) and P0 and other passages (right). The genes which are located in star box represent the ASCs under conditions of log2 (FC.) >4 and -Log10 (adjusted p-value) >5 and enriched terms with an adjusted p-value <0.05 are

reported in the red and blue boxes. (**C**) Principal component analysis (PCA) of time course gene expression profiles. (**D**) Patterns of gene expression by K-means cluster analysis (K=8). K-means clustering of relative expression of all transcripts reveals eight prevalent patterns.

Figure 10

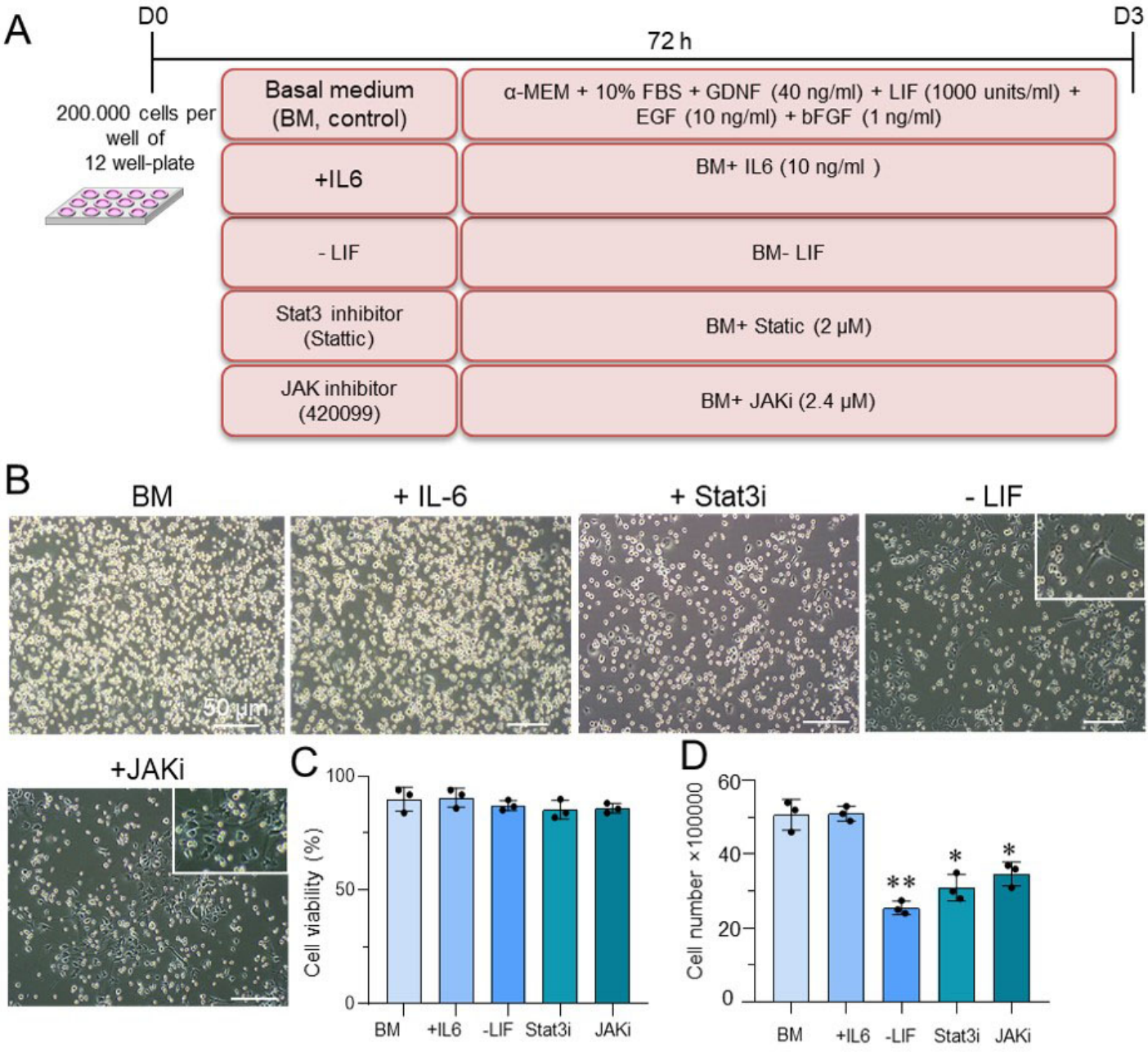

Figure 10

The effect of JAK/STAT3 inhibitor treatment on ASCs derivation.

(**A**) Schema of designed groups to understand the role of the JAK/STAT3 signaling pathway in regulating ASCs pluripotency. (**B**) Phase-contrast picture from ASCs derived in different culture condition for three days. The insets show the morphological transition with higher magnification. (**C, D**) The number and viability of ASCs after three days of culture in different medium. Cells were counted using a hemocytometer after trypan blue staining. Data are means ± SD for three independent experiments. *P<0.05, **P<0.01.

Supplementary Files

This is a list of supplementary files associated with this preprint. Click to download.

- Supplementary.docx
- sup1.png
- sup2.png
- Sup3.png
- Sup4.png
- sup5.png